

Coseismic and postseismic slip distribution of the 2003 $M_w=6.5$ Chengkung earthquake in eastern Taiwan: Elastic modeling from inversion of GPS data

Li-Wei Cheng^a, Jian-Cheng Lee^b, Jyr-Ching Hu^{a,*}, Horng-Yue Chen^b

^a Department of Geosciences, National Taiwan University, Taipei, Taiwan

^b Institute of Earth Sciences, Academia Sinica, Taipei, Taiwan

Available online 22 November 2007

Abstract

The Chengkung earthquake with $M_L=6.6$ occurred in eastern Taiwan at 12:38 local time on December 10th 2003. Based on the main shock relocation and aftershock distribution, the Chengkung earthquake occurred along the previously recognized N20°E trending Chihshang fault. This event did not cause human loss, but significant cracks developed at the ground surface and damaged some buildings. After 1951 Taitung earthquake, there was no larger $M_L>6$ earthquake occurred in this region until the Chengkung earthquake. As a result, the Chengkung earthquake is a good opportunity to study the seismogenic structure of the Chihshang fault. The coseismic displacements recorded by GPS show a fan-shaped distribution with maximal displacement of about 30 cm near the epicenter. The aftershocks of the Chengkung earthquake revealing an apparent linear distribution helps us to construct the clear fault geometry of the Chihshang fault. In this study, we employ a half-space angular elastic dislocation model with GPS observations to figure out the slip distribution and seismological behavior of the Chengkung earthquake on the Chihshang fault.

The elastic half-space dislocation model reveals that the Chengkung earthquake is a thrust event with minor left-lateral strike-slip component. The maximum coseismic slip is located around the depth of 20 km and up to 1.1 m. The slips are gradually decreased to less than 10 cm near the surface part of the Chihshang fault. The seismogenic fault plane, which is constructed by the delineation of the aftershocks, demonstrates that the Chihshang fault is a high-angle fault. However the fault plane changes to a flat plane at depth of 20 km. In addition, a significant part of the measured deformation across the surface fault zone for this earthquake can be attributed to postseismic creep. The postseismic elastic dislocation model shows that most afterslips are distributed to the upper level of the Chihshang fault. And most afterslips consist of both of dip- and left-lateral slip. The model results show that the Chihshang fault may be partially locked or damped near surface during coseismic slip. After the mainshock, the strain, which cumulated near the surface, was released by postseismic creep resulting in significant postseismic deformation.

© 2007 Elsevier B.V. All rights reserved.

Keywords: Coseismic and postseismic deformation; Chengkung earthquake; GPS; Taiwan

1. Introduction

The Longitudinal Valley of eastern Taiwan is a straight, narrow morphological feature separating the high mountains of the Central Range from the Coastal Range. The Longitudinal Valley represents a plate suture between the Luzon arc of the Philippine Sea plate and the Chinese continental margin of the Eurasian plate (Fig. 1a). The NNE-striking Longitudinal Valley fault (LVF), which generally follows the eastern margin of the valley, is an active high-angle oblique reverse fault with a minor left-lateral strike-slip component (Barrier et al., 1982; Liu and Yu, 1990; Lee and Angelier, 1993; Angelier et al., 2000).

Located in the middle to the southern part of the valley, the Chihshang fault is the most active segment of the Longitudinal Valley fault. Along the Chihshang fault, the Lichi Mélange separates the formations of Coastal Range (including also the Takangkou formation of Plio-Pleistocene age and the underlying Tuluanshan calc-alkaline volcanics of the Late Miocene) from the Quaternary alluvial deposits in the Longitudinal Valley (Chang et al., 2000). The surface trace of the active Chihshang fault generally follows the geological and morphological boundary between the hilly Coastal Range to the east and the flat fluvial deposits of the Longitudinal Valley to the west (Fig. 1b). Near the village of Fuli, along a river crossing the fault scarp, the Chihshang fault is exposed with a high dipping angle about 60–70° to the east. The distribution of former micro-earthquakes as well as a few earthquake sequences

* Corresponding author. Tel.: +886 2 33662943; fax: +886 2 23636095.

E-mail address: jchu@ntu.edu.tw (H.-Y. Chen).

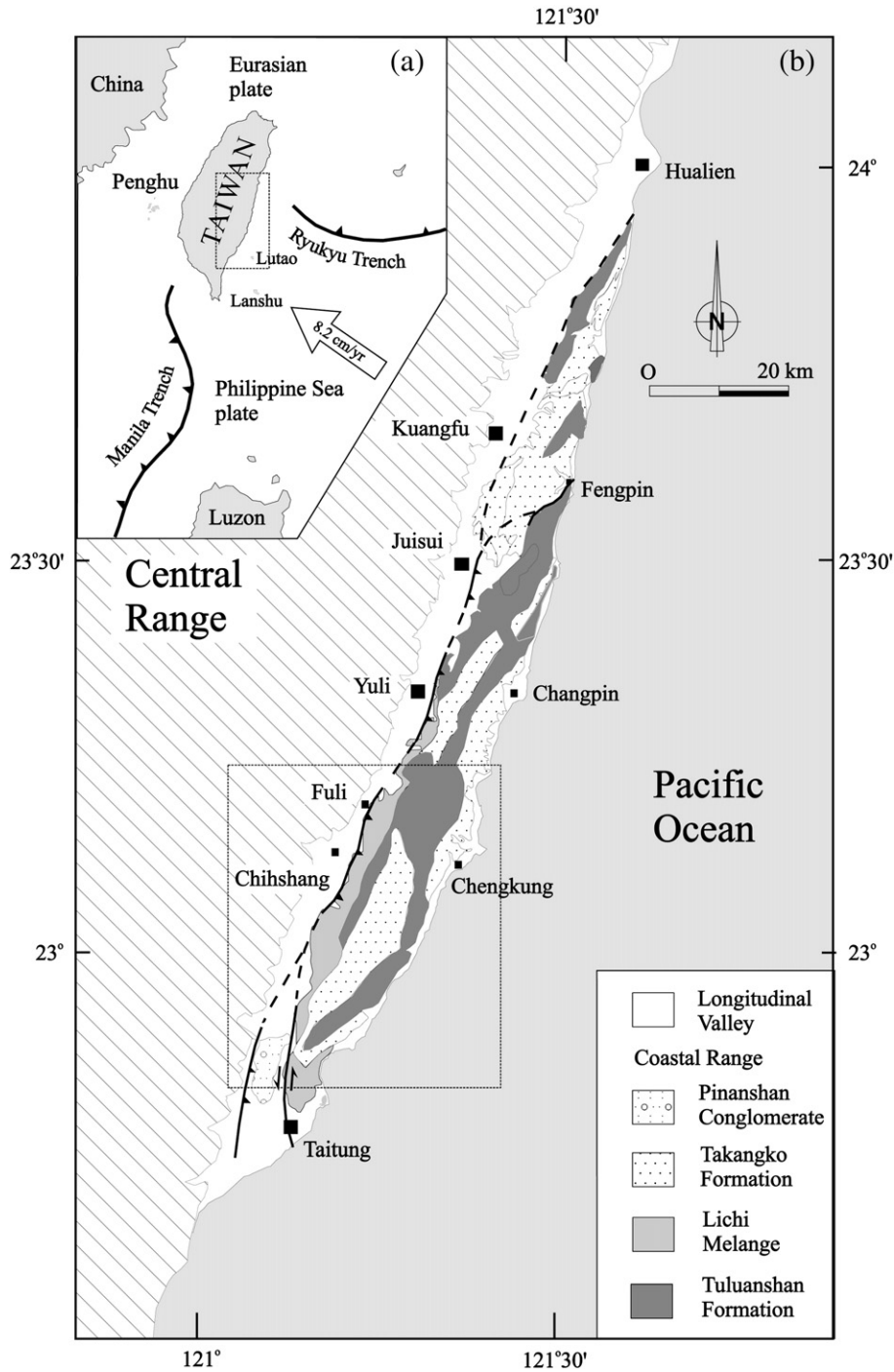


Fig. 1. (a) The tectonic framework of Taiwan. The convergence between Eurasia and Philippine Sea plate is derived from GPS observations (Yu et al., 1999). (b) The simplified geological map of the eastern Taiwan. The Chihshang fault is the most active segment of the Longitudinal Valley fault. In the Longitudinal Valley, the Lichi Mélange separates the formations of Coastal Range from the Quaternary alluvial deposits of the Longitudinal Valley. The surface trace of the active Chihshang fault generally follows a major geological contact between the Pliocene Lichi Mélange to the east (hanging wall) and the Pleistocene–Holocene deposits to the west (footwall).

during recent years suggests that the overall geometry of the Chihshang fault shows a listric shape with a steeper dip angle of about $60\text{--}70^\circ$ at the upper 10 km and becoming gentler to $10\text{--}20^\circ$ at the 20–25 km deep (Chen and Rau, 2002; Lee et al., 2003).

Annual surveys of the GPS measurements along the Chihshang fault during the period 1990–1997 showed a rather

constant horizontal velocity of 3.0 cm/year in a $N40^\circ W$ direction, which accommodates 24% of the total contraction across the Taiwan collision belt (Yu et al., 1990; Angelier et al., 2000; Yu and Kuo, 2001). Geological field investigations also revealed that the Chihshang fault demonstrated a reverse fault motion with left-lateral component, involving fault-perpendicular horizontal shortening of nearly 1.7 cm/year and fault-parallel slip of 1.4 cm/year

(Angelier et al., 1997, 2000). Under this high surface slip rate, the Chihshang fault has experienced creep with significant microseismicities for at least 20 years. Since the last major rupture of the eastern Taiwan earthquake sequence in 1951 ($M_s=7.1$) which resulted in the vertical offsets about tens of centimeters along the

Chihshang fault, there were no big damaging earthquakes occurred in the Chihshang fault area. However, numerous fractures along the fault zone developed during vigorous creep of the fault in the absence of significant earthquakes until 2003. On December 10th 2003, the M_w 6.5 Chengkung earthquake

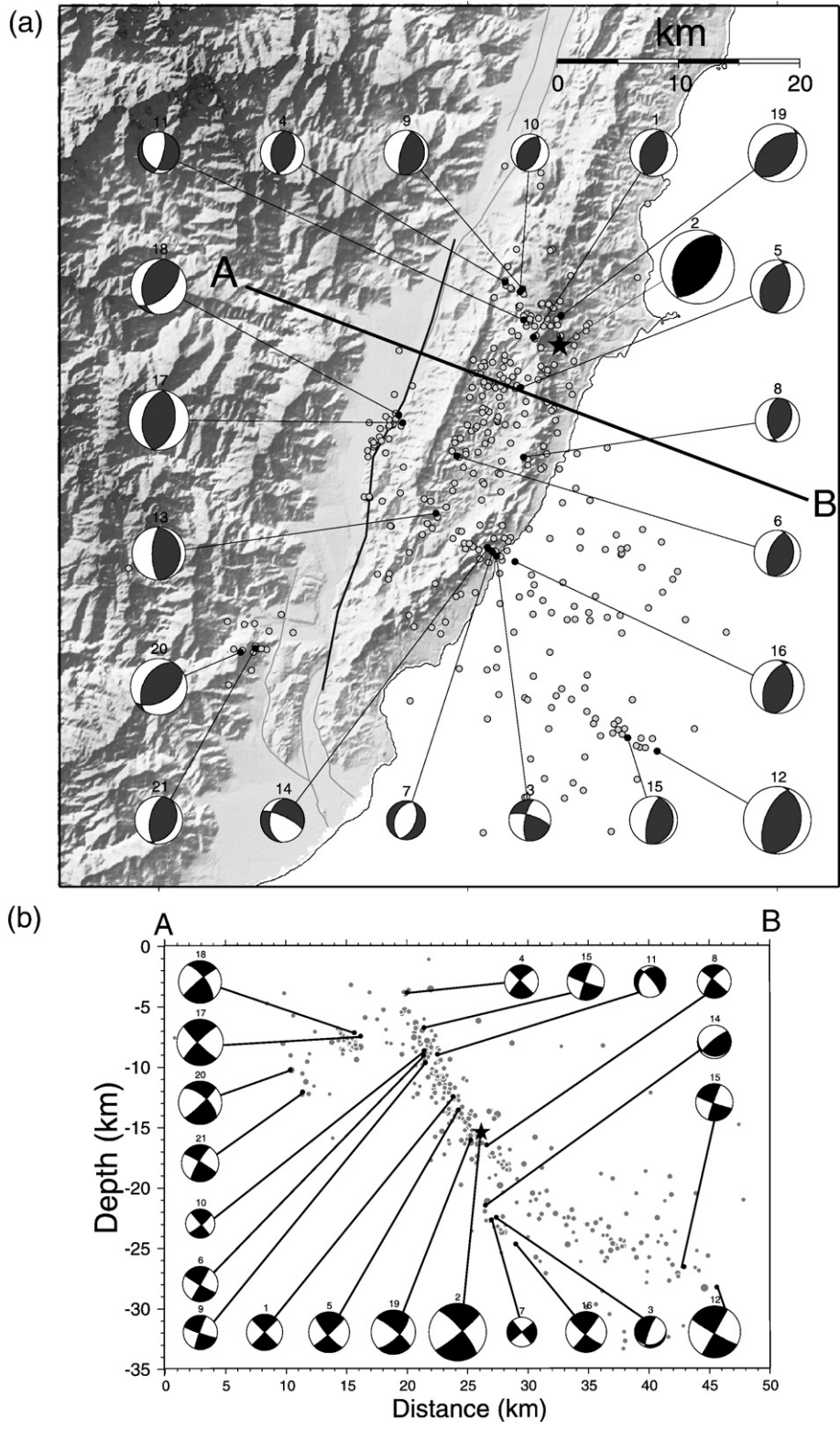


Fig. 2. (a) The fault plane solutions of the Chengkung earthquake and its aftershocks, which mostly reveal inverse events. The asterisk represents the main shock. (b) The profile of A–B in the Fig. 2a demonstrates linear aftershock distribution beneath the Coastal Range.

ruptured from the Chihshang fault. Thus, the behavior of the Chihshang fault is complex and combines with aseismic creep and earthquake slip.

The purpose of this paper aims at the deformation behavior of the Chihshang fault during the 2003 Chengkung earthquake, in particular the slip distribution of the earthquake. We took the GPS measurements as the constraints of the surface coseismic and postseismic deformation to apply the half-space elastic dislocation mechanical behavior, in order to evaluate the slip distribution on the Chihshang fault plane related to the Chengkung earthquake. We also discuss the faulting behavior of the Chihshang fault which caused significant postseismic deformation.

2. Chengkung earthquake

The 2003 Chengkung earthquake, which resulted from a rupture of the Chihshang fault, was located at 23.106°N–121.324°E with a focal depth of 15.7 km (Kuoehen et al., 2004) near the town of Chengkung (Fig. 2a). Following the main shock, thousands of aftershocks occurred and among them eleven $M_L \geq 5$ events took place during the first month. The main shock together with distribution of aftershocks shows a general agreement with the previous defined geometry of the Chihshang fault (Fig. 2b).

In more detail, there are several seismic clusters of the aftershocks (Fig. 2a). A clear linear seismological structure was observed with an east-dipping plane beneath the Coastal Range,

including the main shock, which is consistent with the Chihshang fault plane. However, there are some events away from the Chihshang fault, with focal depth of 7 to 8 km, distributed beneath the Longitudinal Valley. Besides, aftershocks took place in the Central Range with focal depth distributed from 5 to 12 km (Fig. 2b). The focal mechanism solution of the main shock determined by the Finite Dimension Source Model method shows a nearly pure thrust event (Strike=37°, dip=50°, and rake=94°) (Kuoehen et al., 2004). This result is consistent with that of the Harvard CMT solution (strike=10°, dip=51°, rake=69°), with less left-lateral component. According to the focal mechanism solutions, most of aftershocks are thrust types with minor left-lateral component, especially those lie on the listric Chihshang fault plane (Kuoehen et al., 2004). The seismic cluster, which occurred beneath the Longitudinal Valley, also shows the almost pure thrust events.

3. Surface coseismic deformation recorded by GPS

Twenty continuously recording GPS stations and more than 86 campaign-mode survey stations in the Chihshang fault area have been measured and analyzed for monitoring the surface deformation during the 2003 Chengkung earthquake (Chen et al., 2006). The coseismic displacement for continuous stations was determined between the daily solutions, according to the station position time series of the continuously recording GPS stations (Fig. 3). The processing procedure is described in detail

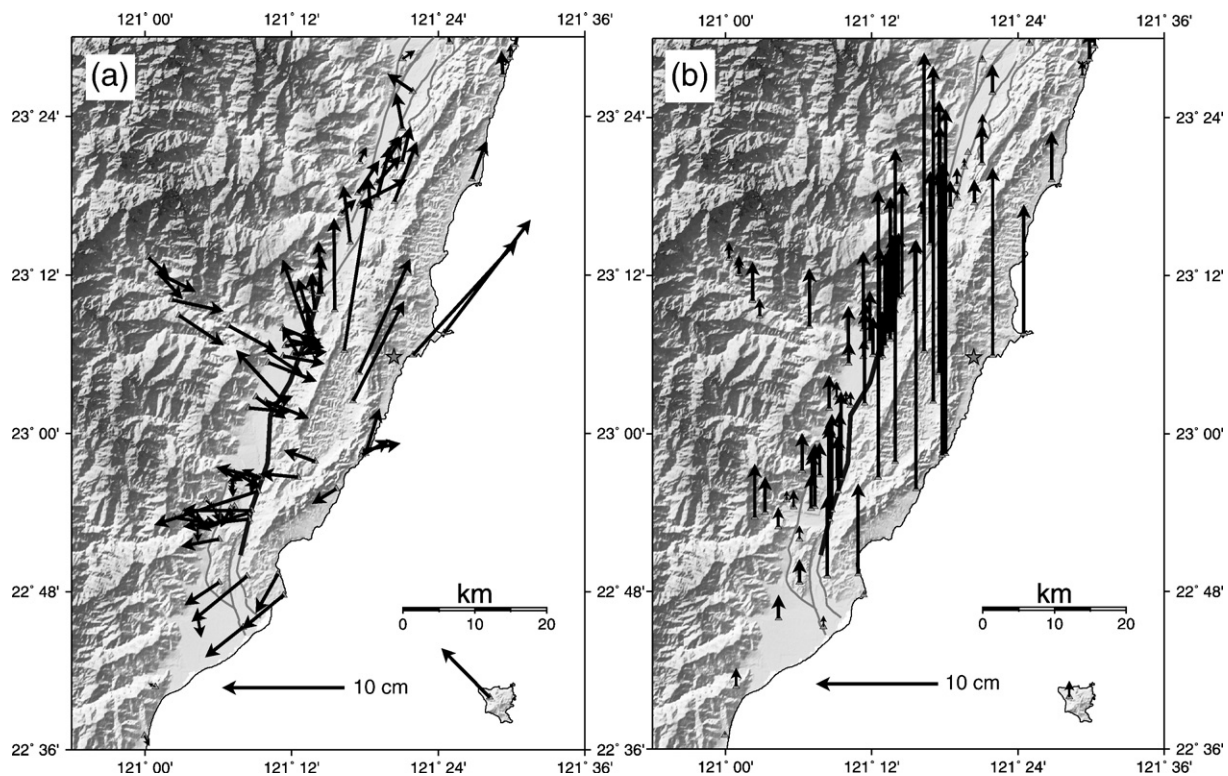


Fig. 3. (a) The horizontal coseismic displacements with 95% confidence ellipses recorded by GPS show a fan-shaped distribution. (b) Vertical coseismic displacements were recorded by GPS. Not only the hanging wall but also the footwall reveals an obvious uplift, up to 29 cm. The red narrow line on the end of the arrow indicates the error bar of vertical displacement. (For interpretation of the references to color in this figure legend, the reader is referred to the web version of this article.)

by Chen et al. (2006). To determine coseismic displacements for the campaign stations, Chen et al. (2006) used the preseismic station velocities (2000–2003) to evaluate the expected station positions on the day of the main shock. The same method was also applied to the correction of nearby continuously recording stations for all campaign-surveyed stations. For modeling in this research, we thus adopted the coseismic displacements determined by Chen et al. (2006) which were used a continuous station (S01R) situated in the stable continental margin in the Taiwan Strait as the reference point.

Significant coseismic displacements have been observed. Concerning the footwall, that is the Longitudinal Valley and the Central Range, the vectors show movements with a fan-shape pattern: towards N or NNE in the north area, towards E or ESE in the middle area, and towards S or SSE in the south area, where the maximum horizontal coseismic displacement is about 4.5 cm (Fig. 3a). As regards the hanging wall, i.e., the Coastal Range, coseismic displacements revealed a clear opposing fan-shape with N or NNE trends to the north, NW or W trends in the middle area and SW trends to the south. The maximum horizontal and vertical coseismic displacements were observed near the epicentral area and reached about 12.6 cm and 26.3 cm, respectively (Fig. 3a). The elevation on the sides of the fault both arose, but varied significant from 1 cm to 30 cm (Fig. 3b).

After the main shock, there are still significant postseismic displacements occurred and were recorded by both campaign-surveyed and continuous GPS stations. The recording span is from 21st Dec. 2003 to 1st Apr. 2004, about 100 days. Larger postseismic

displacements nearly occurred near the surface trace of the Chihshang fault. The maximum uplift of the postseismic movements took place around the Chengkung town about 68 mm. However, the stations on the footwall and on the hanging wall of the Chihshang fault show different manner in coseismic and postseismic displacements (Fig. 4a). With regard to the elevation change of the postseismic movements, the stations near the epicenter moved upward, and other stations moved downward except those near the surface trace of the Chihshang fault (Fig. 4b). The stations located on the hanging wall of the Chihshang fault show the amount of postseismic displacements similar to those of coseismic ones. Alternatively, the stations on the footwall reveal bigger postseismic displacements than coseismic ones.

It seems that the strain had not been totally released by the main shock of the earthquake near surface level along the fault. Hence the postseismic deformation demonstrated a rapid creep around the surface trace of the Chihshang fault during a four-month period (Chen et al., 2006; Lee et al., 2006).

4. Methods

We adopted a Boundary Element Model (BEM), the Poly3D software developed by the Stanford University (Erickson, 1986; Thomas, 1993) for the inversion of coseismic and postseismic surface deformation based on GPS data. The polygonal elements in Poly3D are well-suited for modeling complex surfaces with curving boundaries (Maerten et al., 2005). Fault surfaces which change in both strike and dip can be meshed by triangular

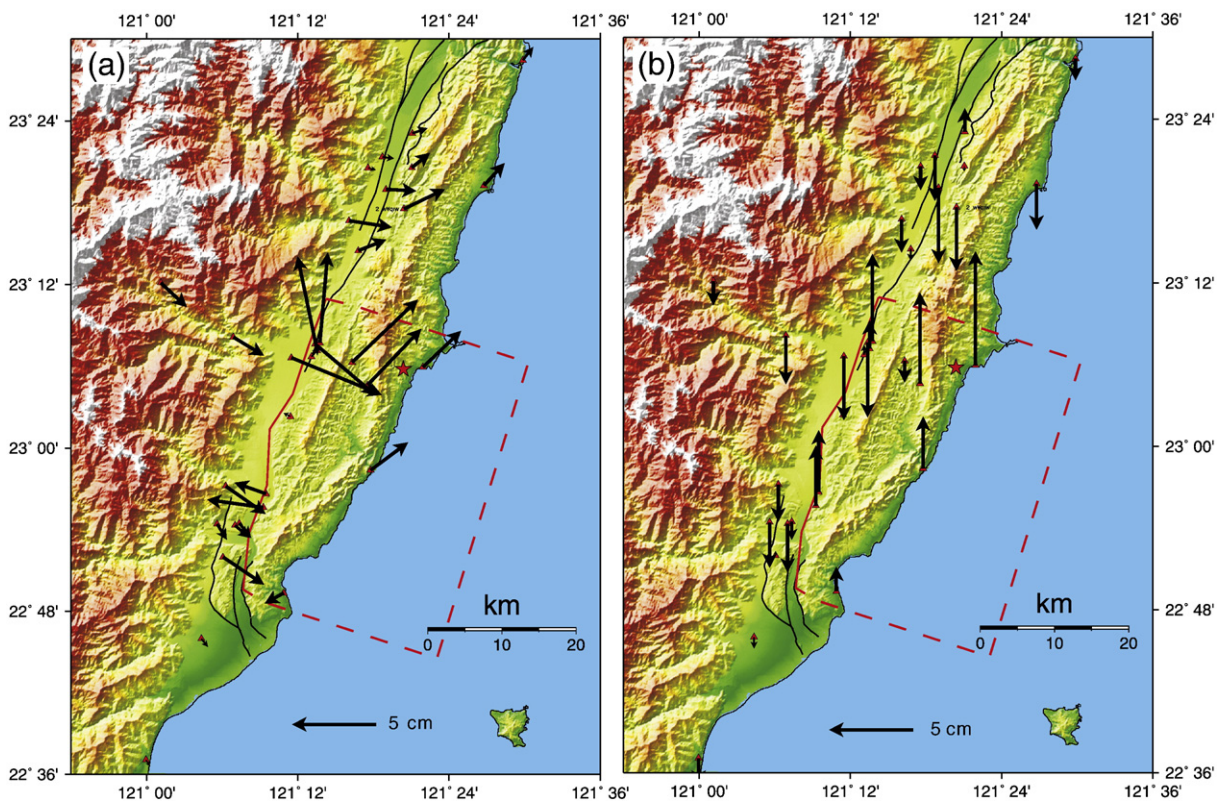


Fig. 4. (a) The horizontal postseismic displacements recorded by GPS of 3 months after the main shock. The GPS stations near the Chihshang fault trace reveal even bigger, up to 7 cm, displacements than coseismic ones. The dashed line means the projection of hypothetical fault plane. The recording span extends from 21st Dec. 2003 to 1st Apr. 2004, about 100 days. (b) With regard to the elevation change of the postseismic movements, the stations near the epicenter moved upward, and other stations moved downward.

Table 1
The geometry of delineation of the aftershocks

	Segment 1 (δ_1)	Segment 2 (δ_2)	Segment 3 (δ_3)	Segment 4 (δ_4)	Segment 5 (δ_5)	Segment 6 (δ_6)
Optimal dip angle	60°	65°	60°	40°	20°	10°
The range of depth (km)	0~6.1	6.1~12.4	12.4~18.5	18.5~23.0	23.0~25.4	25.4~26.6

elements without creating gaps or overlaps. In practice, triangular elements are more flexible for simulating complex geometries than the rectangular elements (Okada, 1985; Johnson et al., 2001). Division of surfaces into triangular elements allows for construction of three dimensional fault surfaces to mimic listric shape and curved tiplines without introducing overlaps or gaps. We use this benefit of triangular elements to construct the Chihshang fault surface.

For describing deformation during earthquake faulting, displacements d_p at points (p) on the Earth's surface due to slip m^e on elements (e) of a buried fault can be described by a set of linear equations:

$$d_p = G^{e,p} m^e + E \quad (1)$$

where E is the observational errors and $G^{e,p}$ is the influence coefficient, or Green's function, that describes how slip on a fault element produces displacement at the Earth's surface. This set of equations can be used to forward model surface displacements from a known fault geometry and slip distribution, or as an inverse problem to model subsurface fault geometry and slip from an observed set of surface displacements. For a given fault geometry, Poly3Dinv can calculate the slip distribution on the fault plane. In practice, the fault geometry is constrained through integration of multiple data sets such as mapped surface ruptures, high-precision aftershocks locations, reflection seismology, and earthquake focal mechanisms.

5. Fault plane reconstruction

According to previous study of relocation of moderate earthquake sequences and micro-seismicity, the Chihshang Fault shows a distinct feature with listric shape beneath the Coastal Range (Chen and Rau, 2002). From the hypocenter of

the main shock, it is obvious that the Chengkung earthquake ruptured from the Chihshang fault and triggered numerous aftershocks around and along the fault. As a result, the Chengkung earthquake and its aftershocks allow us to delineate the seismogenic extent of the Chihshang fault.

The fault geometry is reconstructed by following two criteria: First, the concentrated aftershock distribution in three dimensional space to constrain the dip angle and the length, width of the fault. Second, the fault surface trace, especially the locations of the surface ruptures, is used as a constraint for constructing shallow part of fault plane.

The fault geometry we employ for the numerical model was divided into 6 segments with different dip angle to mimic the aftershock distribution (Table 1). All six segments strike N18°E and change dip angle from 60° at the top near surface to 10° at the bottom at the depth of 25 km (Fig. 5b). The uppermost segment was carefully mapped according to the fault traces of the fault. The optimal fault has 49 vertices constructing 72 isosceles triangular elements (Fig. 5a). The total fault plane of seismogenic area is measured at 1764 km².

6. Numerical modeling of coseismic and postseismic deformation

In our numerical modeling, we assume the fault slipped in a homogeneous, isotropic, elastic half-space, which has been adopted in a variety of geological setting in the world (Okada, 1985; Savage, 1990). The values of elasticity of the crust were adopted by those commonly used in previous work: the Young's modulus 80,000 bars and the Poisson's ratio 0.25. By applying the GPS measurements of the surface displacements and the optimal fault plane with the above mentioned elasticity of rock mechanics, we obtained the coseismic slip distributions of the

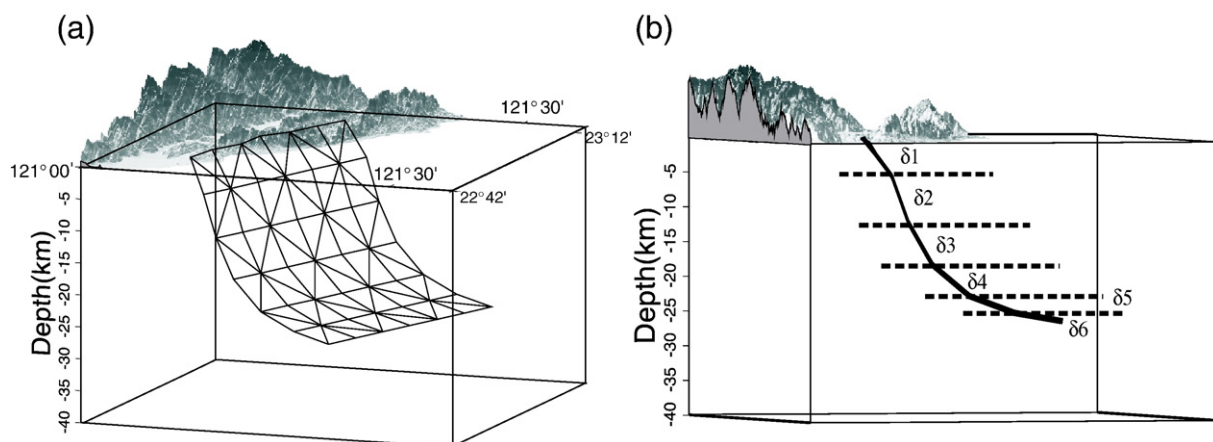


Fig. 5. (a) The 3-dimensional fault geometry used in this dislocation model. The optimal fault has 49 vertices constructing 72 isosceles triangular elements. The total measure of area is 1764 km². (b) The side view of fault geometry. Each dip angle is selected from Table 1.

Chengkung earthquake on the fault plane (Fig. 7). This model-calculated coseismic slip distribution then was applied to yield corresponding coseismic surface deformation. We thus compared this predicted surface deformation to the observed displacements from GPS measurements.

The general trend in net slip of the predicted displacements at the ground surface agrees well with field measurements. In horizontal comparison, the predicted displacements are able to produce two opposing two fan-shaped distributions along the Chihshang fault as revealed by the observed GPS measurements (Fig. 6a). Concerning the amount of deformation, the model predicted displacements generally fit pretty well with the GPS measurements which indicate an increase in net slip from less than 3 cm at the footwall of the Central Range to the maximum value of about 30 cm at the hanging wall of the Coastal Range. The horizontal and vertical RMS (root mean square) misfits are 12 mm and 23 mm, respectively, within the measurement uncertainty. The horizontal angular misfit is 26.8°. As a result, we consider that our elastic dislocation model successfully matches the horizontal GPS data. However, the vertical component seems not to fit well as the horizontal ones.

Concerning the slip distribution, it shows quite uniform rake angles of about 75–85° (Fig. 7) which are consistent with the rake angle estimated from seismic data (Kuochen et al., 2004). In more details, the slip distribution is characterized by reverse rupturing with a minor left-lateral component. In our model calculation, the maximal coseismic slip is up to 110 cm

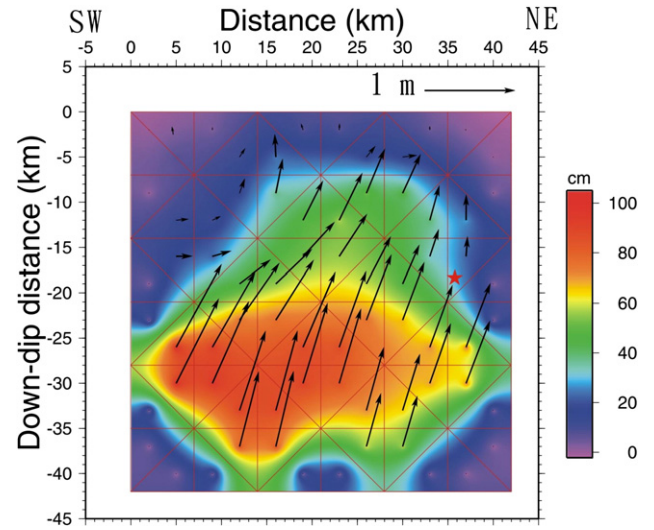


Fig. 7. The overall slip was characterized by reverse rupturing with a minor left-lateral component. The maximum slip is up to 110 cm concentrated at depth of 20 km on the fault. Slips gradually decrease to 7–8 cm at the upper segment near the surface. The average slip is about 52 cm.

concentrated at depth of 20 km. Following the fault plane, the coseismic slip gradually decreases to 7–8 cm at the upper segment near the surface. The average slip on the Chihshang fault patch is about 52 cm (Fig. 7). Therefore, the seismic moment from the geodetic inversion is 2.0×10^{26} dyne-cm sim-

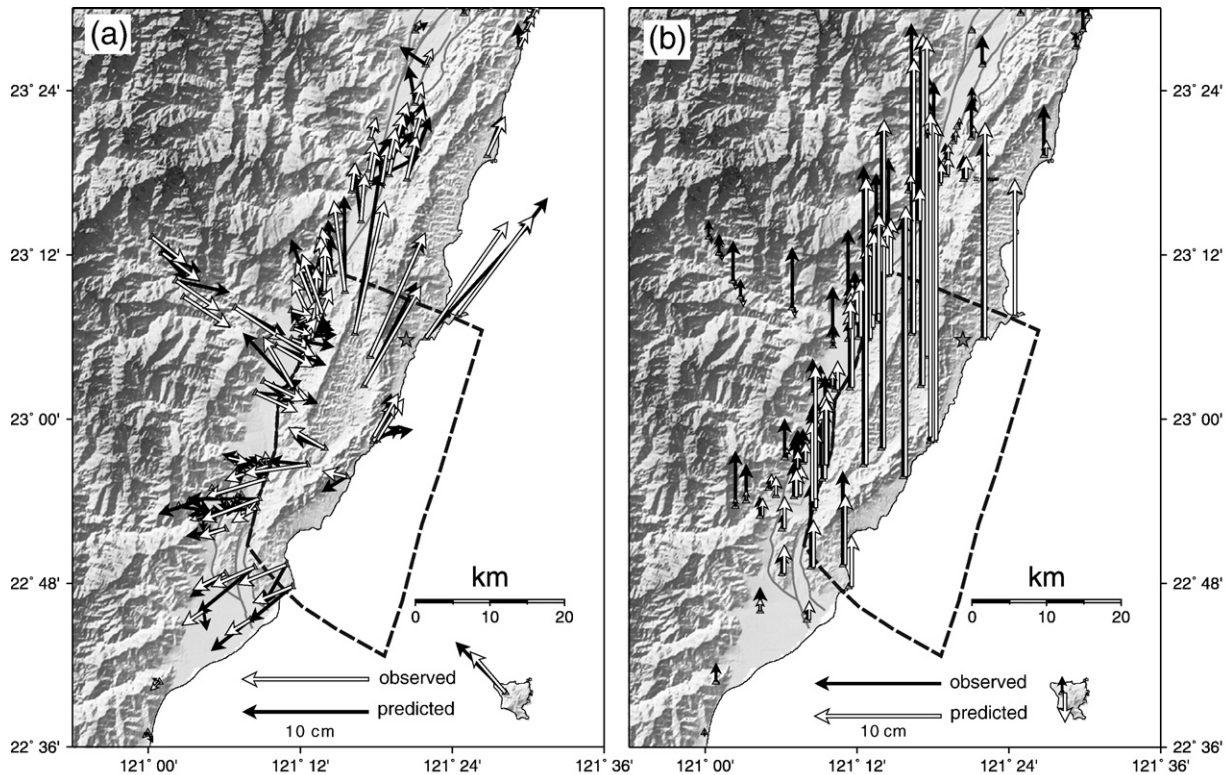


Fig. 6. (a) The comparison between horizontal observed and predicted displacements. The predicted displacements show a fan-shaped distribution as the GPS measurements. The predicted horizontal displacements also indicate an increase less than 3 cm at the footwall of the Central Range to the maximum value of about 30 cm at the hanging wall of the Coastal Range. (b) The comparison between vertical observed and predicted displacements. The predicted vertical displacements do not show a significant uplift of footwall as the GPS measurements.

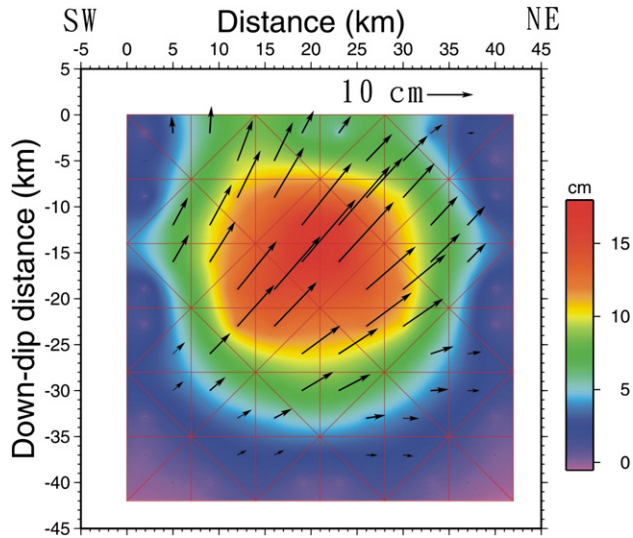


Fig. 8. The postseismic slip was also characterized by reverse rupturing with a minor left-lateral component. The maximum slip is concentrated at depth of 10–15 km on the fault.

ilar with the moments determined by USGS (1.7×10^{26} dyne-cm) and Harvard CMT (2.0×10^{26} dyne-cm). The best fitting double couple representation is in good agreement with the Harvard CMT and CWB solution.

We also carried out an elastic half-space dislocation modeling for postseismic deformation with the same geometry of the Chihshang fault, based on the GPS data during 3 months following the main shock. The result reveals that large postseismic slips of about 5–15 cm were mainly distributed to upper level, in contrast to those of the coseismic stick-slips which distributed at the deeper depth (Fig. 8).

7. Discussion and conclusion

The aftershock distribution reveals a listric fault geometry with high dipping angle ramp near the surface, and becoming a

flat at deeper depth. The geometry of the Chihshang fault, therefore, used in this study is a width and length of 42 km striking $N18^\circ E$ with a variable dip angle depending on the depth (Table 1). The model clearly reveals the location and extent of the major seismogenic source, 20 km and more from the surface along fault dip. The geometry is in agreement with previous researches for the southern Longitudinal Valley fault. The 3-D dislocation model in terms of GPS data demonstrates the maximal dislocation located at the deeper part of the fault is about 1.1 m dip-slip, and the dislocations decrease to 7–8 cm near the surface. This dislocation pattern can be recognized as the displacement pattern on surface because the observed displacements show the maximal displacement on the Coastal Range and gradually decrease to the fault trace as well. The coseismic dislocation model displays that most of coseismic slip are dip-slip with minor left-lateral strike-slip component and it is in agreement with the seismic data (Kuoehen et al., 2004). Despite simplification, this 3-D dislocation model accounts for the general distribution of the coseismic displacements. The RMSs of our model are well within the measurement uncertainty, but some residuals are spatially coherent, especially in the vertical component. The model under-predicts the vertical displacements at 54 of the total 65 (83%) sites on the footwall. This high vertical misfit can be interpreted by two reasons, which one should be the poorer vertical GPS resolution. The GPS vertical resolution is poorer than its horizontal resolution about 2–3 times, as a result, the resolution can highly affect the result of the model and lead to a high misfit consequence. The other reason for high vertical misfit can be explained by the limitation of our elastic, isotropic, homogeneous, half-space model. The model used in this research is conducted under the elastic, isotropic, homogeneous assumption. Due to the significant postseismic deformation and the modeling of postseismic GPS data, we suggest that the Chengkung earthquake did not rupture the upper layers along the fault trace. The strain was cumulated along the upper part of the fault and resulted in the significant uplift of footwall (Fig. 9a). As the time passed by, the cumulative strain was released and caused prominent de-

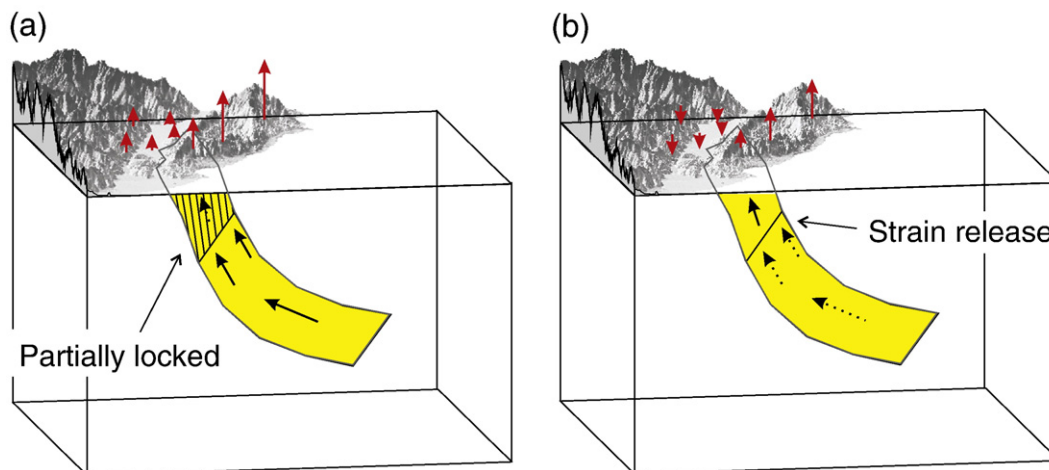


Fig. 9. (a) Coseismic dislocation near the fault trace may be partially locked or damped, thus the strain cumulates. (b) After main shock, the strain released near the surface causes aseismic creeping and significant afterslip.

formation near the surface after the mainshock (Fig. 9b). In sum, our elastic dislocation model leads to consider that the upper layers of the Chihshang fault zone might be temporarily partially coupled, hence prohibiting the propagation of coseismic slippage upwards along the fault. The poorer vertical fit may be due to that the surface rupture during the main shock may not reflect all the sources of postseismic deformation, because some structures activated by the main event may not have surface expression.

Basing on the coseismic dislocation pattern, the large slips are distributed to the deeper part of fault, at depth from 25 to 10 km. On the contrary, that the shallow part of the fault which contributed very little to slip during the Chengkung earthquake experienced significant movement during the 3 months following the earthquake may imply that the faulting of the Chengkung earthquake is not totally ruptured but partially coupled. Consequently, our model under-predicts the uplift of footwall. From this aspect, our model is consistent with the results of local geodetic surveys along the Chihshang fault, which reveals near surface locking of the fault (Chen et al., 2006; Lee et al., 2006). This mechanical behavior, which agrees with the relatively large amount of postseismic displacement along the fault trace in the months following the earthquake, raises influence in terms of seismic hazard. These significant postseismic displacements result from the adjustment of slip along the fault surface in the shallow part of the Chihshang fault. We conclude that the compressive strain had not been totally released, as a probable consequence of the partial locking that affects the shallow part of the active fault zone. Further research will be directed toward the study of coupled effects of the Chihshang fault.

Acknowledgements

We thank editors Benoit Deffontaines and Hsu-Kun Hsu, two anonymous reviewers for constructive comments. We benefited from discussion with Jacques Angelier, Chung-Pai Chang, and Chia-Yu Lu. This research was supported by grants from the National Science Council of Taiwan (NSC 93-2116-M-002-008) and the Central Geological Survey of the MOEA. This research was supported by the Taiwan Earthquake Research Center (TEC) funded through National Science Council (NSC). The TEC contribution number for this article is 00023. Some figures are generated by GMT software written by Paul Wessel and W. H. Smith (Wessel and Smith, 1998).

References

- Angelier, J., Chu, H.-T., Lee, J.-C., 1997. Shear concentration in a collision zone: kinematics of the Chihshang Fault as revealed by outcrop-scale quantification of active faulting, Longitudinal Valley, eastern Taiwan. *Tectonophysics* 274, 117–143.
- Angelier, J., Chu, H.-T., Lee, J.-C., Hu, J.-C., 2000. Active faulting and earthquake hazard: the case study of continuous monitoring of the of the Chihshang Fault, Taiwan. *J. Geodyn.* 29, 151–185.
- Barrier, E., Angelier, J., Chu, H.-T., Teng, L.S., 1982. Tectonic analysis of compressional structure in an active collision zone: the deformation of the Pinanshan Conglomerates, eastern Taiwan. *Proc. Geol. Soc. China* 25, 123–138.
- Chang, C.-P., Angelier, J., Huang, C.-Y., 2000. Origin and evolution of a melange: the active plate boundary and suture zone of the Longitudinal Valley, Taiwan. *Tectonophysics* 325, 43–62.
- Chen, H.-H., Rau, R.-J., 2002. Earthquake locations and style of faulting in an active arc-continent plate boundary: the Chihshang fault of eastern Taiwan. *Eos Trans. AGU* 83 (47) (Fall Meet. Suppl., Abstract T61B-1277).
- Chen, H.-Y., Yu, S.-B., Kuo, L.-C., Liu, C.-C., 2006. Coseismic and postseismic displacement of the 10 December 2003 (Mw 6.5) Chengkung earthquake, eastern Taiwan. *Earth Planets Space* 58, 5–21.
- Erickson, L.L., 1986. A three-dimensional dislocation program with applications to faulting in the earth. M.S. Thesis, Stanford University, Stanford, California, 167 pp.
- Kuo, H., Wu, Y.-M., Chang, C.-H., Hu, J.-C., Chen, W.-S., 2004. Relocation of eastern Taiwan earthquakes and tectonic implications. *Terr. Atom. Ocean.* 15, 647–666.
- Johnson, K.M., Hsu, Y.-J., Segall, P., Yu, S.-B., 2001. Fault geometry and slip distribution of the 1999 Chi-Chi, Taiwan earthquake imaged from inversion of GPS data. *Geophys. Res. Lett.* 29, 2285–2288.
- Lee, J.-C., Angelier, J., 1993. Localisation des déformations actives et traitements des données géodésiques: l'exemple de la faille de la Vallée Longitudinal, Taiwan. *Bull. Soc. géol. Fr.* 164 (4), 533–540.
- Lee, J.-C., Angelier, J., Chu, H.-T., Hu, J.-C., Jeng, F.-S., Rau, R.-J., 2003. Active fault creep variations at Chihshang, Taiwan, revealed by creepmeter monitoring, 1998–2001. *J. Geophys. Res.* 108 (B11), 2528. doi:10.1029/2003JB002349.
- Lee, J.-C., Chu, H.-T., Angelier, J., Hu, J.-C., Chen, H.-Y., Yu, S.-B., 2006. Quantitative analysis of co-seismic surface faulting of the 2003, Mw=6.5 Chengkung earthquake at Chihshang, eastern Taiwan. *J. Geophys. Res.* 111, B02405. doi:10.1029/2005JB003612.
- Liu, C.-C., Yu, S.-B., 1990. Vertical crustal deformations in eastern Taiwan and its tectonic implications. *Tectonophysics* 183, 111–119.
- Maerten, F., Resor, P., Pollard, D., Maerten, L., 2005. Inverting for slip on three-dimension fault surfaces using angular dislocations. *Bull. Seism. Am.* 95 (5), 1654–1665.
- Okada, Y., 1985. Surface deformation due to shear and tensile faults in a half-space. *Bull. Seism. Am.* 75 (4), 1135–1154.
- Savage, J.C., 1990. Equivalent strike-slip earthquake cycles in half-space and lithosphere earth models. *J. Geophys. Res.* 95, 4873–4879.
- Thomas, A.L., 1993. Ploy3D: a three-dimensional, polygonal element, displacement discontinuity boundary element computer program with application to fractures, faults and cavities in the Earth's crust. M.S. Thesis, Stanford University, Stanford, CA, pp 97.
- Wessel, P., Smith, W.H.F., 1998. New, improved version of generic mapping tools released. *Eos Trans. AGU* 79 (47), 579.
- Yu, S.-B., Jackson, D.D., Yu, G.-K., Liu, C.-C., 1990. Dislocation model for crustal deformation in the Longitudinal Valley area, eastern Taiwan. *Tectonophysics* 183, 97–109.
- Yu, S.-B., Kuo, L.-C., Punongbayan, R.S., Ramos, E.G., 1999. GPS observation of crustal deformation in the Taiwan–Luzon region. *Geophys. Res. Lett.* 26, 923–926.
- Yu, S.-B., Kuo, L.-C., 2001. Present-day crustal motion along the Longitudinal Valley Fault, eastern Taiwan. *Tectonophysics* 333, 199–217.